71st International Astronautical Congress (IAC) – The CyberSpace Edition, 12-14 October 2020.
Copyright ©2020 by the authors. Published by the IAF, with permission and released to the IAF to publish in all forms.

IAC-20,C3,4,2,x59999

COMPARATIVE ANALYSIS OF SOLAR POWER SATELLITE SYSTEMS TO SUPPORT A MOON BASE

Drew Gillespie [a], Andrew Ross Wilson [a]*, Donald Martin [a], Gareth Mitchell [a], Gianluca Filippi [a], Massimiliano Vasile [a]

[a] *Department of Mechanical and Aerospace Engineering, University of Strathclyde, James Weir Building, 75 Montrose Street, Glasgow, G1 1XJ, United Kingdom*
* Corresponding Author: andrew.r.wilson@strath.ac.uk

Abstract

This paper compares different concepts for a space-based power system to support a lunar base: a solar power satellite (SPS) with a microwave wireless power transmission system (WPT), a hybrid configuration where two solar reflector satellites (SRS) fly in formation with the SPS and concentrate sunlight onto the SPS, and the CASSIOPeiA SPS system.

Sizing of the transmitting and receiving antennae is conducted for a WPT concept utilising high frequency microwaves. Design of the microwave generator is based on gyrotron technology, with parabolic reflectors, and an array of rectifying patch antennae. The WPT solution consists of a number of satellites with solar arrays and transmission capabilities to provide continuous power to the receiving array.

Solar reflectors alleviate the issue of day-night cycles, for ground-based solar arrays, by providing constant sunlight. This concept could be extended by increasing the irradiance provided by the reflecting satellite, thus decreasing the size of the ground solar array required. However, reflective satellites struggle with efficiency stemming from the size of the footprint they create, which is dependent on the angular subtense of the Sun. This paper demonstrates that a hybrid design, utilizing both the reflector satellites and the WPT, would provide the greatest power to weight ratio - decreasing the size of the solar array required.

An important aspect in the effectiveness of solar powered satellites are their distance from the ground receiver, determined directly by their orbit. Smaller orbits allow for reduced distances between the satellite and ground; reducing receiver sizes. However, larger orbits increase transmission windows, reducing the required energy transfer rate. Another important consideration is the stability of the orbit. Stability is affected by the Solar Radiation Pressure, the gravitational pull of the Earth, and the effects of the non-spherical gravity field of the Moon. Thus, when designing the orbit, these effects have been considered alongside the trade-off between larger and smaller orbits.

The solutions have been scaled and compared to the CASSIOPeiA concept architecture of a similar nature which has been investigated to demonstrate the effectiveness of the concept provided.

Keywords: Solar Power Satellite, CASSIOPeiA, Solar Mirrors, Space Power, Wireless Power Transmission

Acronyms

AU	Astronomical Unit
CFRP	Carbon Fibre Reinforced Polymer
DC	Direct Current
GEO	Geostationary Earth Orbit
ISS	International Space Station
LEO	Low Earth Orbit
PV	Photovoltaic
RCS	Reaction Control System
RF	Radio Frequency
SBSP	Space-Based Solar Power
SPS	Solar Power Satellite
SRS	Solar Reflector Satellite
TRL	Technology Readiness Level
UV	Ultraviolet
WPT	Wireless Power Transmission

1. Introduction

The demand for electrical power is a critical consideration in the design of all space systems. Even more so for crewed missions, the provision of power for habitat and outpost infrastructure such as life support, navigation and communications, as well as supporting scientific research and exploration, is an essential system component and determinant of mission success [1].

These considerations are of great importance for the upcoming Artemis missions - humanity's return to the Moon. Additionally, with plans for longer-term, more sustainable, habitation on the lunar surface, astronauts will require greater magnitudes of power than any space system ever previously deployed [2].

Whilst various technologies have been used to support human space exploration, the most common power systems utilise solar photovoltaic arrays. In space these systems can provide near continuous power

Copyright ©2020 by the authors. Published by the IAF, with permission and released to the IAF to publish in all forms.

generation, with support from on-board battery systems to provide power during periods of eclipse. However, when operating in environments with much longer periods of darkness, such as on the surface of the Moon, the size of the storage systems required to support ground-based solar generation becomes untenable with current technological constraints.

One solution, which has seen increasing study in recent years, is the use of space-based solar power (SBSP) to provide a continuous source of power generation. Originally appearing in the 1941 short story "Reason", by *Isaac Asimov*, the concept of generating solar power in orbit for supply to a ground-based receiver has been studied since the Apollo era of space exploration. The first to address the concept technically, in 1968, was *Glaser* who proposed a system of two satellites operating in geo-synchronous Earth orbit which would harvest solar energy and continuously transmit the converted power via microwave beam [3]. Since then, various concepts for solar power satellites (SPS) have been proposed; addressing different operational environments, mission profiles and technological developments. In particular, the method of wireless power transmission (WPT) and the means of solar energy collection are significant areas of study.

Conceptual SPS systems function via laser or radio-frequency transmission systems, with the latter typically specified as microwave radiation [4]. The transmitted power required at the ground is generated from the conversion of solar radiation into electrical energy by the satellite's solar arrays. Thus, the magnitude of power required and efficiency of the WPT system have great influence over the sizing of the SPS solar arrays, and the WPT antennae. This is important as the solar arrays will constitute a significant proportion of the overall SPS mass, due to their large area; likewise, the area of each WPT antenna will greatly affect the overall mass launched. The direct correlation between cost and mass-launched encourages an optimised design to minimise the size of the solar arrays; with several methods such as advanced solar cell technologies [5], ultralight-weight structures [6] and concentration of solar radiation [7] having previously been explored in literature.

2. Background

As part of the Swiss Space Centre's IGLUNA 2020 project, in this investigation a system-level approach is undertaken, to study, scale and compare different designs and configurations for an SPS constellation. As such, the aim of this work was to produce a single design which is capable of providing continuous power to a lunar outpost at the Moon's south pole. The study focuses mainly on currently available technologies with readiness level (TRL) equal to, or greater than, TRL 3 with a view toward near-term deployment in order to support ESA in their goal of building a permanent Moon base.

2.1 IGLUNA 2020

Inspired by the *Chandrayaan-1* probe's discovery of water ice at the lunar south pole, the IGLUNA project is an international collaboration of student teams to develop concepts and prototypes to support human exploration on the Moon [8]. The current work derives from concepts explored by the authors, members of the PowerHab student team, as part of the 2020 project edition.

Tasked with the goal of a reliable and continuous power supply for the lunar base, the PowerHab team developed a distributed and holistic solution to meet this objective. The design consisted of multiple subsystems for energy generation, storage and distribution to allow for redundancy should one subsystem fail. As the main generation element, SBSP was a key component of the overall power system and is the only element defined within the scope of this work.

2.2 PowerHab Requirements and Constraints

System requirements and constraints were specified at the outset of the study with definition of power budgets for each team's system, review of existing spacecraft power systems and projection of future demand.

The key technical requirements (R) and constraints (C) of the PowerHab system within scope are outlined below in Table 1:

Table 1: Key Design Requirements and Constraints

R.1	Power at Habitat	150 kW
C.1	Diameter of WPT Transmitter	≤ 22 m
C.2	Diameter of WPT Rectenna	≤ 400 m

Required power delivered to the habitat was specified as 150 kW. This was derived by comparison to the International Space Station (ISS) power system of 110 kW [2, 9], with a 40% margin applied after review of the total power budget of the other teams' systems.

Constraint *C.1* was determined from the largest diameter antenna reflector ever deployed, the *SkyTerra-1* which has an L-band reflector diameter of 22 m [10, 11]. Constraint *C.2* was established upon preliminary review of the WPT method, with microwave transmission chosen for study due to its level of efficiency and demonstrated heritage of terrestrial and space technologies operating in the microwave spectrum.

Using a nominal areal density of 0.16 kg/m^2 [12] for the rectenna, and using an approximate upper mass limit of 26,000 kg (based on the injected mass of the Orion spacecraft to provide a baseline [13]), one derives an area of 160,000 m^2 which equates to an effective diameter of 400 m for a square array rectenna.

In addition to these requirements and constraints, an objective was defined to size the system for minimised mass whilst adhering to the design boundaries.

Copyright ©2020 by the authors. Published by the IAF, with permission and released to the IAF to publish in all forms.

3. Orbital Analysis

Under ideal conditions, any orbit would remain stable and unchanged indefinitely, without the need for any 'station-keeping' manoeuvres. However, in reality several effects perturb orbits over time. The main effects considered here are third body effects, non-spherical gravity fields, and solar radiation pressure.

Third-body effects, such as the Earth-Moon-Satellite system, occur where a satellite in orbit around the Earth is affected by the gravitational attraction of the Moon, causing perturbations in its original orbit. In this analysis the three-body system considers only the Earth affecting the orbit of a proposed satellite around the Moon.

Non-spherical gravity fields can arise due to the body not being perfectly spherical in shape, but they can also occur due to the effects of "mascons"; which are large concentrations in mass causing gravitational anomalies across the surface. This is the case for the lunar surface.

The final effect considered in this project is the effect of solar radiation pressure (SRP). Due to wave-particle duality, an electromagnetic photon has an amount of momentum, which can be imparted upon an object that the photon collides with. In reflectors, the photon will be reflected, sometimes in the exact opposite direction, potentially doubling the effect of the 'radiation pressure' compared to a surface which absorbs the photons.

Frozen orbits, which are sometimes possible through the careful selection of initial orbital parameters, could theoretically keep a satellite in the desired orbit indefinitely, eliminating the need for station-keeping manoeuvres, meaning less maintenance, fuel, and cost associated with the operation of the satellite.

One study states that a lunar orbit with semi-major axis of 6541.4 km, inclination of 56.2^0 and eccentricity of 0.6 will be frozen [14]. The third body effect of the Earth is considered to be the main source of perturbation and discounts the effect of the non-spherical gravity field as negligible due to the large semi-major axis.

NASA has demonstrated that orbits with inclinations of 27º, 50º, 76º, and 86º around the Moon are frozen [15], when considering the non-spherical gravity field as the primary source of perturbation. These are close to the lunar surface, which minimises the WPT distance.

One effect not considered in either study is SRP, which is significant in the perturbation of a SBSP system; and varies across the solar year, not just across the orbit. However, in the case of satellites with relatively high mass, in low lunar orbit, the effect of SRP is essentially negligible.

To assess the stability, orbit simulations were conducted and variation in the orbital parameters were studied. The first method used was a 3D MATLAB simulation. Initially desired Orbital parameters were input and converted to cartesian coordinates in a state vector. The magnitude and direction of the force of gravitational attraction of both the Moon and the Earth were determined by using the pre-defined gravitational parameters of each and the distance between the satellite and the respective body's centre of mass using Eq. 1, where the mass of the satellites were negligible.

$$F = \frac{Gm_1m_2}{r^2} \qquad \text{Eq. 1}$$

By superposition, the accelerations from each body were summed to find the total acceleration due to gravity. Using the direction of the sun relative to the satellite, and by determining whether the satellite was experiencing an eclipse, the force acting on the satellite due to SRP was calculated. Acceleration due to this force was calculated and added to the gravitational acceleration to determine the overall acceleration of the satellite at that point in time. Effects on the position and velocity due to the current acceleration and velocity were calculated over a time step of one second, with acceleration values recalculated for every time step and simulated over a 5-year period. Notably, this method does not determine effects of the non-spherical gravity field, which is of major influence for low lunar orbits. For this purpose, a second simulation method was used utilising NASA's General Mission Analysis Tool (GMAT).

With GMAT, the non-spherical gravity field of the Moon could be modelled, and its effects taken into account; improving the accuracy and reliability of the results. The in-built tools of GMAT were used to extract the variation in parameters over the simulated 5-year period and track the eclipses experienced by the satellite.

Four orbit paths were simulated over the 5-year period to provide a comparison of the orbit stability, eclipse time, coverage times, and altitude. The stable 6,500 km orbit mentioned previously; a larger version of the orbit for comparison; a low lunar orbit, with inclination of 86°, to determine the effectiveness of the satellite orbiting very close to the surface; and a circular polar orbit with a semi-major axis of 2250 km. The selected orbits' parameters are given in Table 2, followed by visualisations of each orbit in Figure 1.

Table 2: Orbital Parameters Investigated

Orbit No.	***a*** *(km)*	***e***	***i*** *(°)*	**Ω** *(°)*	**ω** *(°)*	**T** *(hr)*
1	**1880**	0.025	86.0	90	90	2.04
2	**2250**	0	90.0	90	90	2.66
3	**6514**	0.600	56.4	90	90	13.06
4	**9250**	0.600	56.4	90	90	22.17

Copyright ©2020 by the authors. Published by the IAF, with permission and released to the IAF to publish in all forms.

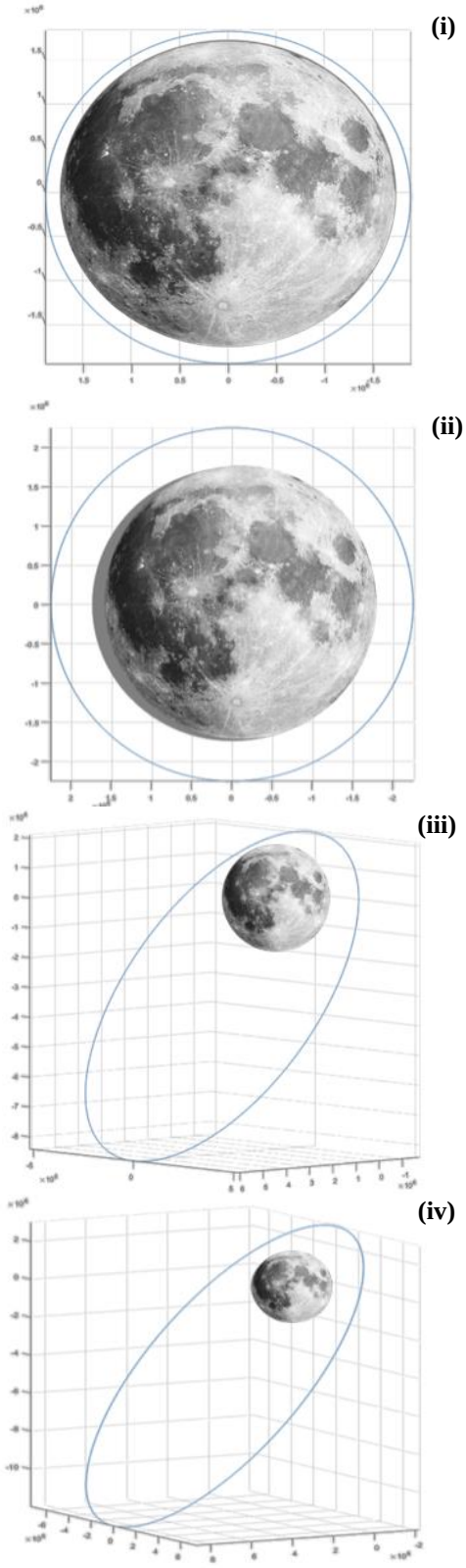

Figure 1: Visualisations of Lunar Orbits (i) *No. 1,* (ii) *No. 2,* (iii) *No. 3 and* (iv) *No. 4*

4. Wireless Power Transmission

Following the decision to employ a microwave transmission system, explained in Section 2.2, the frequency of the microwave beam was chosen as 94 GHz based on literature review of similar systems [16, 17]. This corresponds with a wavelength of 3.189 mm.

Taking a conservative RF-to-DC conversion efficiency of 40% [18, 19, 20], the power required at the WPT rectenna was determined by:

$$P_r = \frac{P_{hab}}{\eta_{RFDC}} \qquad \text{Eq. 2}$$

The area and mass of the rectenna array, composed of microstrip patch antennae, could then be evaluated by Eq. 3 using the average rectenna power density, S_r, and an areal density of 0.16 kg/m^2 [12].

$$A_r = \frac{P_r}{S_r} \qquad \text{Eq. 3}$$

Thus, S_r can be treated as a fundamental physical property of the individual rectenna, for a given transmission frequency and RF collection efficiency, to scale the sizing of the rectenna array.

Continuing with this methodology for an RF collection efficiency of 93% [16], the size of the transmitter required was then determined by:

$$\eta_{RF} = 1 - e^{-\tau^2} \qquad \text{Eq. 4}$$

$$\tau = \frac{\sqrt{A_t A_r}}{\lambda d} \qquad \text{Eq. 5}$$

where λ is the wavelength of the microwave beam, and d is the distance between the transmitting and receiving apertures [21].

For our purposes, the transmitter consists of two elements: the antenna reflector and the oscillating source. The size of the antenna reflector was the area denoted by A_t. For this study a Cassegrain parabolic reflecting antenna, with area density equal to 1.4 kg/m^2 [22] and efficiency of 80% [23], was incorporated due to its high TRL, efficiency and suitability for operation at the required frequency.

Choice of oscillator was determined by the microwave frequency and output power required, illustrated below in Figure 2. In accordance with the 94 GHz frequency of the beam, and power requirement *R.1* from Table 1, a gyrotron was the only oscillator capable of supplying the intended system. From the comparable sources available, mass of the gyrotron was taken to be ~800 kg [24, 25, 26], with an efficiency of 40% [27, 28].

Copyright ©2020 by the authors. Published by the IAF, with permission and released to the IAF to publish in all forms.

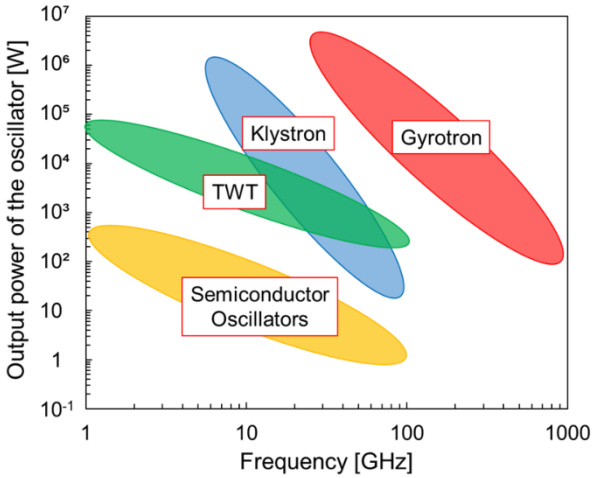

Figure 2: Oscillator Output Power for Range of Frequencies [17]

As discussed in Section 1, the electrical input power required for the transmitter is crucial in the sizing of the SPS solar array. The magnitude of this power was calculated by Eq. 6, where η_{DCRF} is the efficiency of the DC-to-RF conversion of the transmitter.

$$P_{t_{in}} = \frac{P_r}{\eta_{RF} * \eta_{DCRF}} \qquad \text{Eq. 6}$$

5. Solar Power Satellite

As previously mentioned, sizing of the SPS solar array is a core element in the estimation of the mass of the overall satellite system. For this reason, work was directed towards the optimal design and trade-off analysis of the solar blanket and support structure.

Before any significant design work could be conducted on the overall array, a trade-off analysis was undertaken on choice of the solar cell, with the following options by AZUR SPACE investigated:

Table 3: Solar Cells Analysed [29]

Cell	***Junction Type***	***Efficiency Class***	***Composition***
S 32	Single	17%	Cz Si
3G28C	Triple	28%	GaInP/GaAs/ Ge
3G30C	Triple	30%	InGaP/GaAs/ Ge
4G32C	Quad	32%	AlInGaP/ AlInGaAs/ InGaAs/Ge

Sizing of the solar array began with derivation of the power required to be produced, given by P_{array} in Eq. 7.

$$P_{array} = \frac{\frac{P_e T_e}{X_e} + \frac{P_{t_{in}} T_a}{X_a}}{T_a} \qquad \text{Eq. 7}$$

This was calculated using the solar array energy balance outlined in [30], where T_a and X_a denote the access time with the rectenna and losses within coverage window; and subscript e denotes the parameters during eclipsed conditions. Losses given by the parameter X included those attributable to satellite's harness, batteries, latching current limiters and battery charging and discharging regulators.

The area of the array required was then evaluated using the cell specific power, P_{cell}, which incorporates pointing accuracy, cell degradation, packing factor and incident solar irradiance:

$$A_{array} = \frac{P_{array}}{P_{cell}} \qquad \text{Eq. 8}$$

Following on from this, the mass of the solar blanket required was thus:

$$M_{blanket} = A_{array} * \dot{m}_{cell} \qquad \text{Eq. 9}$$

where $\dot{m}_{cell}$ is the cell specific mass, taken from the data sheets of the AZUR SPACE cells analysed.

Estimation of the structural support mass of the array followed the methodology outlined in the NASA-led study of a high-power solar electric propulsion space tug [31]. The array was divided into 2 'wings', with each 'wing' sub-divided into 8 'winglets' – illustrated in Figure 3 below. Dimensions b and h of each winglet, shown in Figure 4, were then evaluated from:

$$b = \sqrt{\frac{3}{128} * A_{array}} \qquad \text{Eq. 10}$$

$$h = \frac{8}{3} * b \qquad \text{Eq. 11}$$

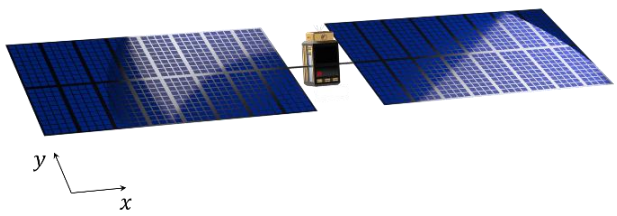

Figure 3: Visualisation of SPS without microwave transmitter (not to scale)

Copyright ©2020 by the authors. Published by the IAF, with permission and released to the IAF to publish in all forms.

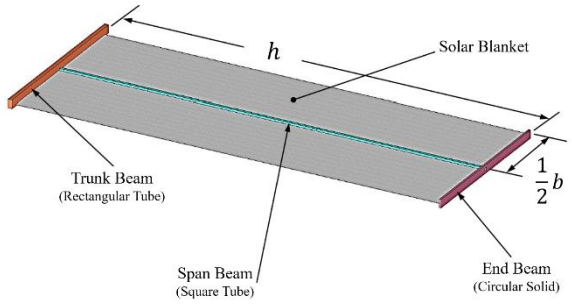

Figure 4: Single solar array winglet [31]

Mass of the support structure, $M_{structural}$, was then estimated from the volume of the structural members:

$$V_{trunk} = 8b * A_{trunk} \quad \text{Eq. 12}$$

$$V_{span} = 16h * A_{span} \quad \text{Eq. 13}$$

$$V_{end} = 16b * A_{end} \quad \text{Eq. 14}$$

where the density values from Table 4 below were used during the trade-off analysis of the materials.

Table 4: Structural Materials Sampled [32, 33]

Material	**Density** (kg/m^3)	***Yield*** *(MPa)*	***Young's Modulus*** *(GPa)*
CFRP	1550	800	150.0
Stainless Steel	7850	585	199.5
Low Alloy Steel	7850	950	211.0
Aluminium	2700	290	75.0
Titanium	4600	975	115.0
Ni Super Alloy	8200	1100	197.5

As such, the total mass of the SPS was then determined by:

$$M_{SPS} = 1.3 * \left(M_{array} + M_t\right) + M_{Other} \quad \text{Eq. 15}$$

where a 30% margin was applied to estimate the structural mass of the satellite bus and mechanisms, according to [30], and M_{Other} represents the cumulative mass of the satellite's other sub-systems, calculated according to [34].

6. Solar Reflector Satellite

The fundamental concept behind reflective satellites is that they are mirrors in orbit which reflect the sun's rays; and are used to increase irradiance on an object or to illuminate shadowed areas. The mirrors can either be flat or concave, which focuses the rays. Since reflective satellites are relatively light compared to solar cells, it is more efficient to increase the solar irradiance on a solar cell than to increasing the number of cells when requiring an increase in power. However, problems arise when reflecting sunlight over large distances, such as orbital altitudes.

The angular subtense, α, which denotes the angle between the sun and the orbital reflector, shown in Figure 5, causes the satellite's reflected footprint to expand. The area of the footprint can be simplified into two equations, representing the two different scenarios. Eq. 16 is the footprint area for a flat reflector. Whereas Eq. 17 describes the footprint if the mirror is focused on a point, where h is the orbital height above the solar cells and A_r is the area of the reflective surface. From these equations the impact of the angular subtense on the footprint is clear; as is the exponential expansion of the footprint with an increased orbital height, for increased access time, which is not beneficial.

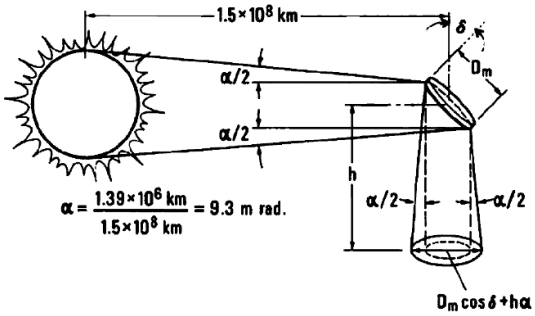

Figure 5: The depiction of a solar reflector and the surrounding variables [35]

$$A_f = A_r + \frac{\pi}{4}(\alpha h)^2 \quad \text{Eq. 16}$$

$$A_f = \frac{\pi}{4}(\alpha h)^2 \quad \text{Eq. 17}$$

Eq. 18 describes the irradiance which the mirror imparts onto a surface where I_f is the irradiance in the footprint, ρ is the mirrors reflectivity and C is the cloud factor ranging from $C = 1$ *(cloudless)* to $C = 0$ *(extremely cloudy with no light penetrating)*. The angle δ is that between the reflected beam and the mirror's normal, θ is the angle between the incident and reflected beams and I_s is the solar constant at 1AU, which for the purpose of this work is taken to be 1367 W/m^2. The function $f(\mathcal{E})$ describes the reduction of irradiance due to the haze and zenith distance, where $\mathcal{E}$ is the angle above the horizon to the orbital reflector. In this work, the equation can be simplified because the reflector will be orbiting the Moon at a high enough altitude to exclude haze and zenith effects, as shown within Eq. 19.

Copyright ©2020 by the authors. Published by the IAF, with permission and released to the IAF to publish in all forms.

$$I_f = \rho C \frac{A_r}{A_f} f(\varepsilon) cos\delta \cos\left(\frac{\theta}{2}\right) I_s \qquad \text{Eq. 18}$$

$$I_f = \rho \frac{A_r}{A_f} cos\delta \cos\left(\frac{\theta}{2}\right) I_s \qquad \text{Eq. 19}$$

The $\frac{A_r}{A_f}$ term becomes very important when considering scaling, since this ratio has a large effect on the footprint illumination. Since A_f is predominantly dependant on the distance to the solar cell, A_r is required to be approximately the same size or larger. This results in two possible outcomes: a cluster of smaller reflectors, or one very large reflector.

The membrane must have a low area density as the reflective area could be kilometres squared, most proposed designs work with an areal density of 3 g/m^2 to 6 g/m^2. Earlier proposed materials were aluminised Kapton or Paralene [36]. However, more recent designs have focused on aluminised Mylar with a UV protective coating [35]. The penetration depth of solar particles is approximately 0.1μm, thus it is required that the reflective material be at least this thick. The membrane will also be subjected to UV radiation which causes degradation in polymers due to photochemical reactions taking place between the bonds. Most damage would be sustained by the first 0.3μm from the illuminated surface, as this is the attenuation depth of UV. To ensure bulk properties of the polymer film are not affected, the minimum thickness should be 0.3μm [35].

Other external factors which affect the membrane are micrometeorites, space debris, and solar winds. The *ECHO-I* satellite, which had 12.5μm Mylar coated with 0.22μm of aluminium, lost 4.7% reflectivity over the course of 4 years. The Boeing Company estimated that a solar sail in GEO would result in a reduction of 3% reflectivity over 30 years from micro meteorites. Less confidence is present when predicting the sputtering erosion and hydrogen effects. However, Boeing believe that a satellite requiring no maintenance for up to 8 years could be achievable, although this requires further testing [36]. *Billman et al* suggested an in-situ technique which could extend the life reflectors by recoating the mirror. They suggest a metal evaporator, placed at the end of each boom, periodically reevaporate a replacement coating. This would mean that degradation would only be dependent on micrometeorite and polymer substrate damage [36].

Minghong's work on thin film coatings gave a rough estimate on reflectivity of the aluminium coating and proposed a dielectric layer to enhance the aluminium base. At a wavelength of 1064 nm the hybrid coating of Al-$(SiO_2/HfO_2)_3$ had a reflectivity of 99.1% and was 0.68μm thick – an improvement of 4.1% compared with the pure aluminium [37]. A similar experiment was conducted by *Barron*, and the results are displayed in Figure 6. The pure Aluminium had a steep drop off below 450 nm. However, the aluminium copper alloys only fluctuated between 86% and 91% across the visible light range [38].

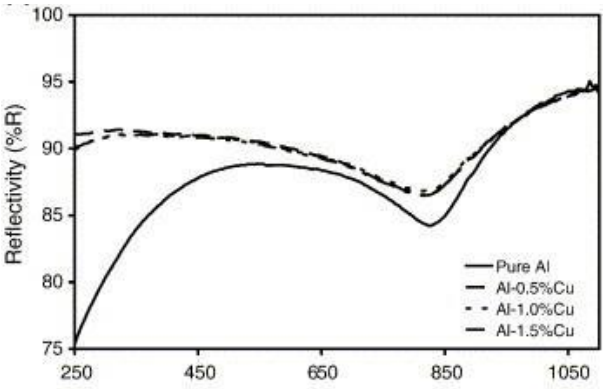

Figure 6: Reflectivity of Aluminium Alloys [38]

A hybrid design combining the orbital reflectors and the SPS system would help increase the power to mass ratio of the SPS system, as it will decrease the size of solar array required. The concept requires two reflector satellites which reflect the sunlight in a "Z" fashion but still allowing the SPS system direct sunlight as, well as shown in Figure 7. The only limiting factor to the irradiance that this design can impart onto the SPS is the heat dissipation by the solar panels. For this concept to be efficient the additional mass of the cooler for the solar panels and mirrors must be less than the mass of the solar array removed.

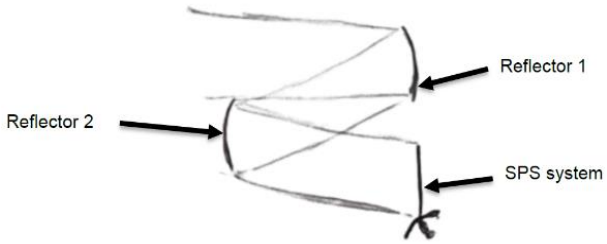

Figure 7: Hybrid Concept Reflection Paths

The design for the satellite will be similar to the *L'Garde solar sail* comprising of 4 inflatable beams webbed with the membrane [39]. The middle of the satellite will be the core and be the case for the deflated reflector with the sunwards facing side covered with solar cells to generate the require power. The orientation will be controlled by reaction wheels allowing for expulsion free control, as RCS waste could contaminate the reflective surface. The preliminary design for this satellite is displayed in Figure 8.

Copyright ©2020 by the authors. Published by the IAF, with permission and released to the IAF to publish in all forms.

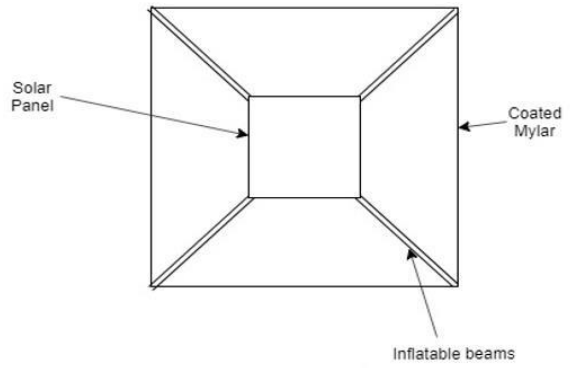

Figure 8: Reflective Satellite Preliminary Design (Not to Scale)

The mass of the satellite is required to be relatively low. To achieve this the beams will be made from Aluminium and Mylar, similar to the *Inflatesail* design [40]. The beam is a sandwich of 16μm of mylar surrounded by two 14.5μm sheets of Aluminium. This means that a beam of 90 mm diameter will mass around 2.3 g/m. The beam is inflated by pressurised nitrogen to 70 kPa, which plastically deforms the creases that occurred from folding. The visual results from the *Inflatesail* test are displayed in Figure 9. The beams have a structural rigidity of 5.6×10^{-4} Nm and an estimated Youngs modulus of 68 GPa. The beams have a compression ratio of around 6% meaning that a 10m beam will start off around 60 cm long.

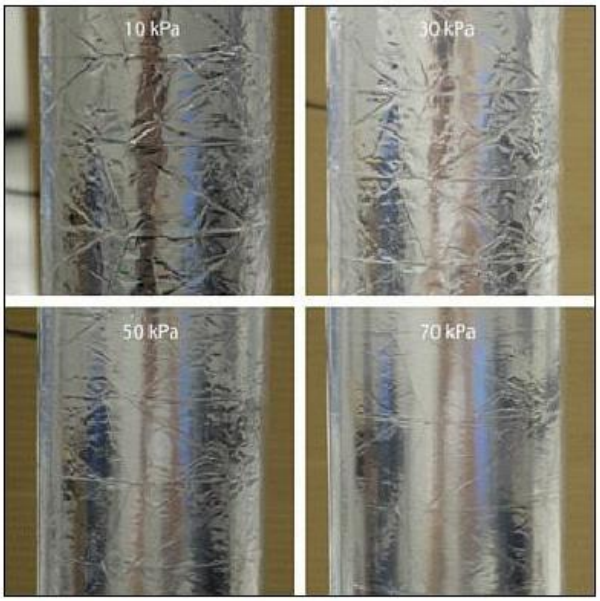

Figure 9: Inflatesail pressurisation test [40]

The membrane will be 2.2μm Mylar coated by 0.35μm of aluminium, it is hoped that the thicker aluminium coating compared with the *ECHO-I* satellite will help slow down the blistering process allowing the satellite to last around 10 years, however, exact estimates will require physical testing. This will give the membrane an areal density of 4 g/m^2 which is in between the requirements proposed by *Billman* [36].

7. Results

The results of each analysis have been conducted to derive specifications of the SPS, WPT and SRS systems. Comparison between the SPS concept and a hybrid concept including both SPS and SRS are then presented.

7.1 Orbit Comparison

The results of the orbital analyses, shown in Appendix A – Orbital Analysis Results, demonstrate that the closer orbits are more affected by the non-spherical gravity field of the Moon than the third-body effect of the Earth, which is shown by the difference between the two simulation results for Orbit 1 as the MATLAB code does not consider the non-spherical gravity field. However, the results for the simulation methods are very similar for Orbits 3 and 4, where the main perturbation comes from the third body effect of the Earth. In addition to this, the GMAT simulation uses a specific epoch of the year 2025, whereas the MATLAB simulation uses a specific setup of the satellite, Moon, Earth, and Sun, where they all start along a straight line.

From the results summarised in Table 5, below, it was determined that the coverage time for the low lunar orbit, Orbit 1, was very short at times leaving less room for error in the transmission of the power. This makes it less reliable and, in the case of requiring continuous coverage of the ground base, an unreasonable amount of satellites would be required.

Table 5: Satellite Coverage and Eclipse Analysis

Orbit		***Coverage***		***Eclipse***	
No.	***a*** *(km)*	***Min. t*** *(hr)*	***d*** *(km)*	***Max.*** *(hr)*	***Avg.*** *(hr)*
1	**1880**	0.10	150- 633	1.91	0.80
2	**2250**	0.45	512 – 1158	2.25	0.75
3	**6514**	9.40	5571 – 9008	1.02	1.00
4	**9250**	22.17	7656 - 13392	1.33	1.19

Orbit 1 is also more susceptible to changes in the orbit causing instability that would result in a crash of the satellite, which must be avoided in the case of delivering electricity to the ground base that is necessary to sustain the lives of the inhabitants. The rest of the orbits were deemed to be feasible, with Orbit 2 giving a reasonable compromise for the altitude of the satellites, however it also has the largest maximum eclipse duration which would be an important factor in design of the satellite. It

Copyright ©2020 by the authors. Published by the IAF, with permission and released to the IAF to publish in all forms.

must also be noted that the solar radiation pressure will have an effect on the orbit path over time and that regular station-keeping manoeuvres will be required to keep the satellite in orbit for an extended period of time. This affects Orbit 2 more than 3 or 4 as it is polar, and the effect can be seen from the results of the MATLAB code simulation. As Orbit 4 is essentially a larger version of Orbit 3, if Orbit 3 was deemed to be more suitable than Orbit 2, then the impact of the larger orbit on the transmission distance would be the main factor in considering which orbit to use.

7.1.1 WPT Considerations

Further evaluation of the feasibility of each orbit was conducted with the WPT element. Two 'MinMax' cases were studied: minimisation of the receiver (maximising transmitter) and minimisation of the transmitter (maximising receiver). The results of this analysis are outlined in Table 6 and Table 7 respectively.

Table 6: Orbit Analysis for Receiver Minimisation

a *(km)*	***S_r*** *(W/m^2)*	***Transmitter***		***Receiver***	
		D_t *(m)*	***M_t*** *(kg)*	***D_r*** *(m)*	***M_r*** *(kg)*
1880	13.153	22	1332.2	168.85	4561.825
2250	3.9300	22	1332.2	308.90	15,266.81
6514	0.0650	22	1332.2	2402.9	923,821.4
9250	0.0294	22	1332.2	3572.3	2,041,842

Table 7: Orbit Analysis for Transmitter Minimisation

a *(km)*	***S_r*** *(W/m^2)*	***Transmitter***		***Receiver***	
		D_t *(m)*	***M_t*** *(kg)*	***D_r*** *(m)*	***M_r*** *(kg)*
1880	2.3438	9.28693	894.834	400	25,600
2250	2.3438	16.9896	1117.37	400	25,600
6514	2.3438	132.159	20,004.9	400	25,600
9250	2.3438	196.478	43,246.8	400	25,600

As previously noted, Orbit 1 *(a = 1880 km)* was deemed unfeasible due to potential instabilities over time. Additionally, results from the analysis above demonstrate that even in the best-case scenarios of each antenna, Orbits 3 and 4 would require prohibitively massive transmitting or receiving antenna in terms of diameter and mass respectively. Thus, Orbit 2 *(a = 2250 km)* clearly offered the best solution.

7.2 WPT Receiver Power Density

Studying Orbit 2 for a range of receiver power density values yielded the plot seen in Figure 10 below. Here the diameter of the receiver and transmitter are plotted within the range defined by requirements *C.1* and *C.2*, which correlate with $S_r = 3.93\ W/m^2$ and $S_r = 2.3438\ W/m^2$ respectively. This provides a power density range in which to determine an optimal trade-off between the sizing of the receiver and transmitter. Furthermore, conducting this analysis for mass instead of diameter yields Figure 11, demonstrating the linear proportionality between receiver power density and transmitter mass, and inverse proportionality between receiver power density and receiver mass. Thus, variation of the receiver power density value has a greater impact on the sizing and mass of the receiver.

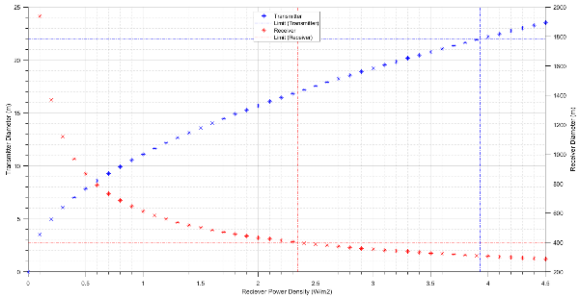

Figure 10: Antenna Diameter for a Range of Receiver Power Densities

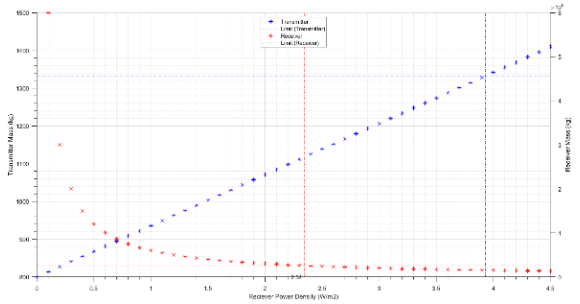

Figure 11: Antenna Mass for a Range of Receiver Power Densities

The optimal receiver power density, $*S_r$, over the entire feasible range can thus be found from $min(\Delta M)$ by applying:

$$dM_t = |M_t - \min(M_t)| \qquad \text{Eq. 20}$$

$$dM_r = |M_r - \min(M_r)| \qquad \text{Eq. 21}$$

$$\Delta M = |M_r - M_t| \qquad \text{Eq. 22}$$

where $\min(M_r)$ and $\min(M_t)$ represent the minimum values within their respective sets.

Conducting this analysis for an increasing resolution, outlined in Table 8, allows for an accurate determination of $*S_r$.

Copyright ©2020 by the authors. Published by the IAF, with permission and released to the IAF to publish in all forms.

Table 8: Convergence of Optimal Receiver Power Density

No. of Data Points	S_r (W/m^2)
1.00E+01	3.930093532
5.00E+01	3.86663979
1.00E+02	3.882503226
1.00E+03	3.877744195
1.00E+04	3.877426926
1.00E+05	3.877347609
1.00E+06	3.877350782
1.00E+07	3.877351099

The aforementioned yields a solution of $*S_r = 3.8774\ W/m^2$, accurate to 5 significant figures. This represents a balanced approach to the trade-off, with the use of mass magnitude providing a slight bias towards minimisation of the receiver size; which is beneficial due to receiver's greater impact on the mass of the overall system.

Re-evaluating the parameters of the WPT element using the optimal receiver power density determined results in the final specification outlined in Table 9.

Table 9: Final WPT Breakdown

	Mass *(kg)*	***Diameter*** *(m)*	***Area*** *(m^2)*
Transmitter	1322.55	21.80	373.25
Receiver	15,465.41	310.90	96,658.81

7.3 SPS

7.3.1 Solar Array Comparisons

A sub-system level analysis was conducted to evaluate the solar blanket mass and area required for each solar cell type studied. These results are shown below.

Table 10: Solar Cell Trade-Off

Cell Type	***Blanket Mass*** *(kg)*	***Area*** *(m^2)*
S 32	3100.55	9689.23
3G28C	6310.35	5439.96
3G30C	4470.79	5198.60
4G32C	8526.03	4789.90

From the results above, the **S 32** cell clearly resulted in the lowest blanket mass required. However, the low efficiency of the single-junction silicon crystal resulted in the largest area required. This is significant as the much larger area could pose issues with volumetric constraints of a payload fairing and would also result in a disproportionate support structure mass. Thus, the optimal cell type was determined to be the **3G30C**, which provided a balanced solution, with the second lowest mass and area results.

The mass of the support structure required for the array was then analysed for the materials listed in Table 4, with Table 11 displaying the results of the overall structural mass when each beam is made of the same material.

Table 11: Support Structure Material Trade-Off

Material	***Mass*** *(kg)*	***Young's Modulus*** *(GPa)*
CFRP	5555.1	150.0
Stainless Steel	28133.8	199.5
Low Alloy Steel	28133.8	211.0
Aluminium	9676.6	75.0
Titanium	16486.1	115.0
Ni Super Alloy	29,388.2	197.5

The greater strength-to-weight ratio of the CFRP results in lowest overall mass of the support structure. When also considering the intrinsic stiffness of the materials analysed, important for the trunk and span beams which support structural loads, CFRP was determined to be the best material due to its low mass, high strength and moderately high stiffness properties.

7.3.2 Overall System Specification

Incorporating the results determined in the previous sections, the final specification of the SPS provided below in Table 12.

Table 12: Final SPS Breakdown

	Mass *(kg)*	***Area*** *(m^2)*
Solar Array	10,025.88	5198.60
Transmitter	1322.55	373.25
Other	6729.80	–
Total	*18,078.23*	–

For continuous coverage, an SPS system at an orbit with semi-major axis of 2250 km requires a 6-satellite constellation. Thus, the mass breakdown for the overall system is:

Table 13: Overall System Mass Breakdown

	SPS	***Receiver***	***Overall System***
Mass *(kg)*	18,078.23	15,465.41	123,934.79

7.4 Hybrid System

7.4.1 SRS Specification

As stated previously the solar reflectors will be positioned in a "Z" fashion with the angles incident to reflected rays being very small ~2°. Reflector 1 (as named in Figure 7) will be 8.9 km from Reflector 2,

Copyright ©2020 by the authors. Published by the IAF, with permission and released to the IAF to publish in all forms.

which will be 4.9 km away from the SPS' solar array. Using the material and structure discussed previously working with Eq. 19, one reflector satellite would have the following specifications;

Table 14: SRS Specifications

Reflective Area	5281m^2
Areal Density	4g/m^2
Minimum Reflectivity	0.85
Reflective Irradiance	3kW/m^2
Mass	~46kg

Each reflector is curved with a focal point equalling the distance between the satellite and illuminated object. Because of the angular subtense of the sun this still allows for the whole object to be illuminated while also concentrating the irradiance.

Even though the total area is around 5.3×10^3 m^2 each beam only starts off at 3.08 m allowing for a simple launch.

7.4.2 System Comparison

The "Z" formation allows the SPS arrays to be irradiated from both the reflectors and from direct sunlight. This design provides a total irradiance on the PV cells of just over 4.4 kW/m^2, an increase of 220%. Since the Solar Reflectors are much lighter than the PV cells they replace, this leads to a big reduction in weight.

As described earlier the SPS and WPT system has a mass of 18.08 tonnes when used by itself with the array size required being almost 5200 m^2. The benefits of the hybrid system become clear when the increased irradiance on the array allows its area to be reduced to 1609 m^2.

Table 15: Final SPS Breakdown for Hybrid Concept

	***Mass** (kg)*	***Area** (m^2)*
Solar Array	4474.95	1609.4
Transmitter	1322.55	373.25
Other	7850	–
Total	*10,584.47*	–

This reduces the SPS mass to only 10.58 tonnes. Considering the two SRS required to achieve this, the final mass of the hybrid concept is 10.67 tonnes. Therefore, the hybrid system saves 7.40 tonnes per SPS, which is 44.41 tonnes over the whole constellation.

Table 16: Overall System Breakdown for Hybrid Concept

	SPS	***SRS***	***Receiver***	***Overall System***
***Mass** (kg)*	10,584.47	46	15,465.41	79,524.23

When the systems are compared side to side, as shown in Table 17, the benefits the hybrid concept has becomes clear. The hybrid concept increases the power per kilogram by almost 50% which is important when considering the scalability. The reduction in array size also reduces complications which occur with very large arrays, such as, volumetric issues when launching, increased difficulties with dual access tracking and increased risk of micrometeorite damage. However, the hybrid concept comes with some drawbacks, such as requiring the launching, monitoring, and control of three times the amount of satellites. Because of the launch costs involved with launching to lunar orbit the Hybrid concept is the better choice as it is two thirds the weight of a pure SPS system.

Table 17: SPS and Hybrid Concept Comparison

	SPS	***Hybrid***
No. of Satellites	6	18
***PV Area** (m^2)*	5198.6	1609
***Power** (kW)*	150	150
***Mass** (tonnes)*	123.9	79.5
***Specific Power** (W/kg)*	1.21	1.89

8. Comparison with CASSIOPeiA System

To examine the effectiveness of the PowerHab solution, the system was compared to the state-of-the-art CASSIOPeiA concept; with consideration of each system's suitability for the lunar mission profile.

8.1 CASSIOPeiA Background

CASSIOPeiA is a novel concept for a fully solid-state SPS system. The satellite's helical structure, shown in Figure 12, uses concentrated PV and forms a microwave phased array transmitter with constant aperture [41]. The solid-state design eliminates the need for moving parts, yet also avoids redundancy of the generation and transmission components, thereby reducing mass [42].

Figure 12: CASSIOPeiA SPS variant with 1-sun quadrant planar reflectors [42]

Copyright ©2020 by the authors. Published by the IAF, with permission and released to the IAF to publish in all forms.

8.2 Comparative Analysis

Whilst comparison between the PowerHab and CASSIOPeiA systems must be undertaken with some caution, due to the differences in operational factors, it is worthwhile to compare some key figures of merit to examine how each system could be improved by attributes of the other.

Table 18: Proposed CASSIOPeiA Mission Profiles [41]

	Near Space	***LEO***	***GEO***
***Altitude** (km)*	7 - 20	963 - 7414	35786
***Power** (kW)*	100 - 200	90,000	430,000
***Mass** (tonnes)*	0.2 – 0.4	90 - 180	400 - 900
D_t *(m)*	34	650	1430
D_r *(m)*	74	1450	3160

Study of proposed CASSIOPeiA mission profiles, found in Table 18, indicate the most similar orbital profile to the PowerHab concept to be the LEO constellation. Comparison between similar orbital profiles is more significant than power magnitudes due to the effects of increasing transmission distance.

Table 19: Key Figures of Merit for Comparison

	PowerHab	***CASSIOPeiA***
***Altitude** (km)*	512 - 1158	963 - 7414
Specific Power (W/kg)*	2.34	~500
S_r *(W/m²)*	3.88	62.07

****Note:** Not including mass of rectenna*

From the worst-case LEO configuration, derivation of the specific power and rectenna power density, listed in Table 19, demonstrate the CASSIOPeiA system to be greater than an order of magnitude more capable than the PowerHab system in both categories.

Despite these results highlighting the fact that PowerHab may be an inferior system, it is important to consider additional factors which affect the suitability of each system in meeting the near-term objectives if they are to be applied as part of IGLUNA.

In this regard, the IGLUNA project's directive is to support development of an ESA lunar base. For this reason, systems with high TRLs are preferable in order to meet ESA's goal of lunar habitation within the next decade. Additionally, the overall configuration of the PowerHab system's satellites are highly comparable to existing systems such as the ISS (with respect to the solar arrays, for the SPS) and the LightSail-2, IKAROS and NanoSail-D2 small satellites for the SRS. Conversely, despite components of the CASSIOPeiA system being comparable to those of PowerHab; namely the solar cells and reflectors; the overall configuration and scale of the structure has no measurable precedent for comparison. Additionally, whilst the helical design theoretically enables compact stowage, the complexity of this structure increases the number of potential mechanisms of failure during deployment.

It must also be stressed that CASSIOPeiA has so far only been detailed and proposed for Earth applications. The further analysis required to accurately examine the feasibility and operation of CASSIOPeiA within cislunar space would increase pre-launch period and delay deployment of the system.

Considering the overall combination of proven technologies and comparability to existing systems, the timescale required to test and deploy the PowerHab system is more feasible in achieving the targets set by ESA when compared to the CASSIOPeiA system. However, given its properties for Earth applications, if a longer-term revision was made to these targets then the CASSIOPeiA system would likely provide a better solution.

9. Conclusions

This paper has analysed and compared several design options and system concepts to provide a feasible space-based solution for continuous power supply to a lunar base. Comparison of viable orbits and system architectures was conducted, with trade-offs analysed for the solar array and wireless power transmission elements.

The final concept consisted of a hybridised solution incorporating SPS and SRS to reduce the overall mass of the system by 44.24 metric tonnes – making this concept not only feasible but economic.

This hybrid solution was then compared to the novel CASSIOPeiA design. Given the ESA target of a near-term lunar base, the PowerHab system was deemed a more achievable solution due to its readiness comparability to existing systems. However, it was noted that CASSIOPeiA would potentially prove a better solution if this target was delayed.

Acknowledgements

The authors would like to thank Samuel Beard, Alex Potter, Gavin Rodgers, Finlay Rowe, Bradley Skelton and RS Components for their support and contributions to the IGLUNA 2020 project. This work was supported by the Swiss Space Centre under the European Space Agency's ESA_Lab@CH initiative.

Copyright ©2020 by the authors. Published by the IAF, with permission and released to the IAF to publish in all forms.

Appendix A – Orbital Analysis Results

A.1 - Orbit 1

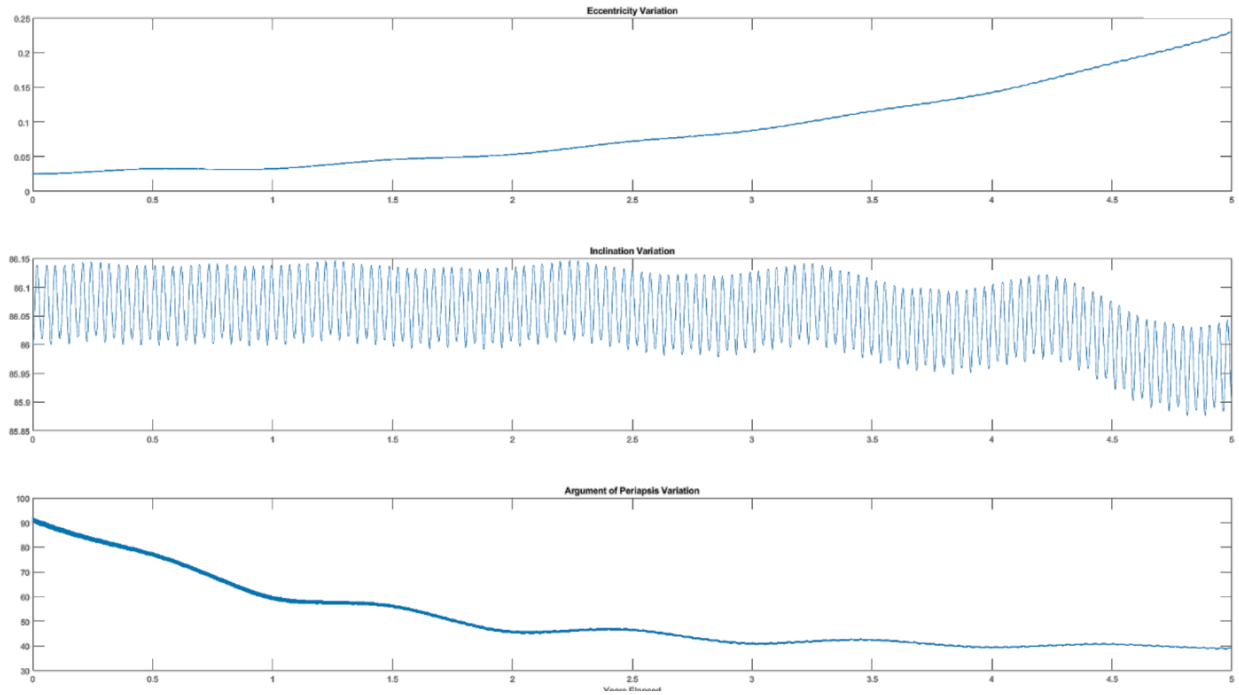

Figure 13: MATLAB Simulation of Orbital Parameter Variation for Orbit 1

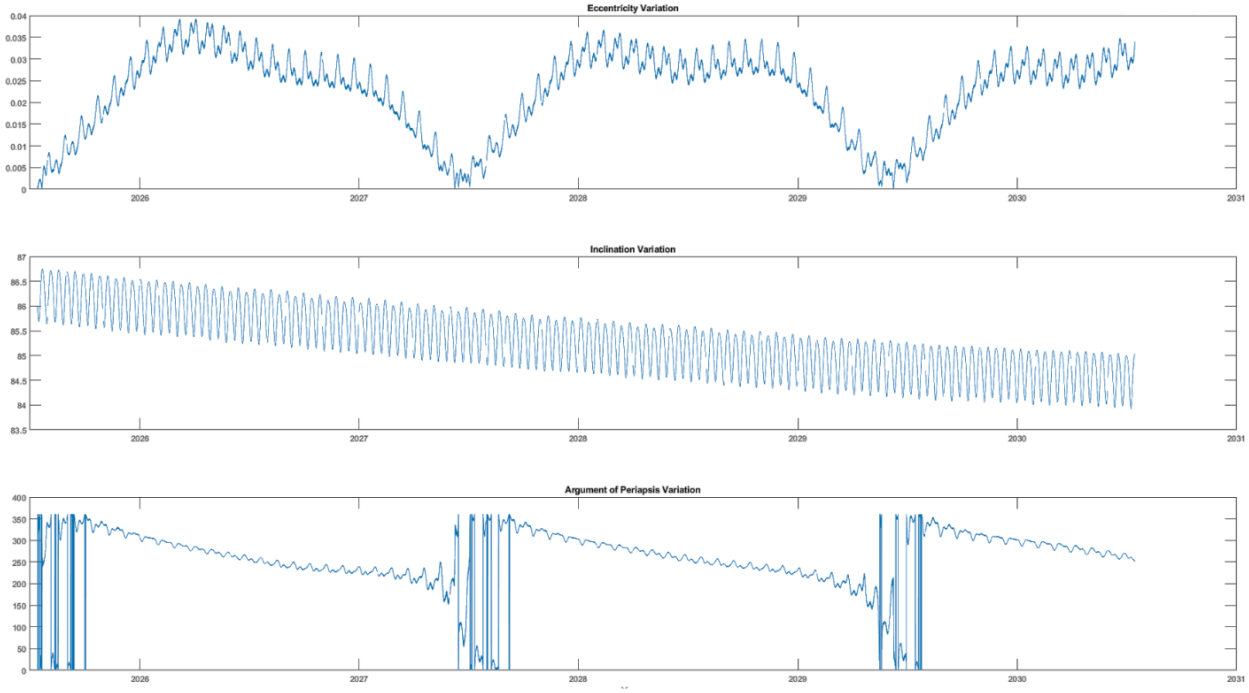

Figure 14: GMAT Simulation of Orbital Parameter Variation for Orbit 1

Copyright ©2020 by the authors. Published by the IAF, with permission and released to the IAF to publish in all forms.

A.2 - Orbit 2

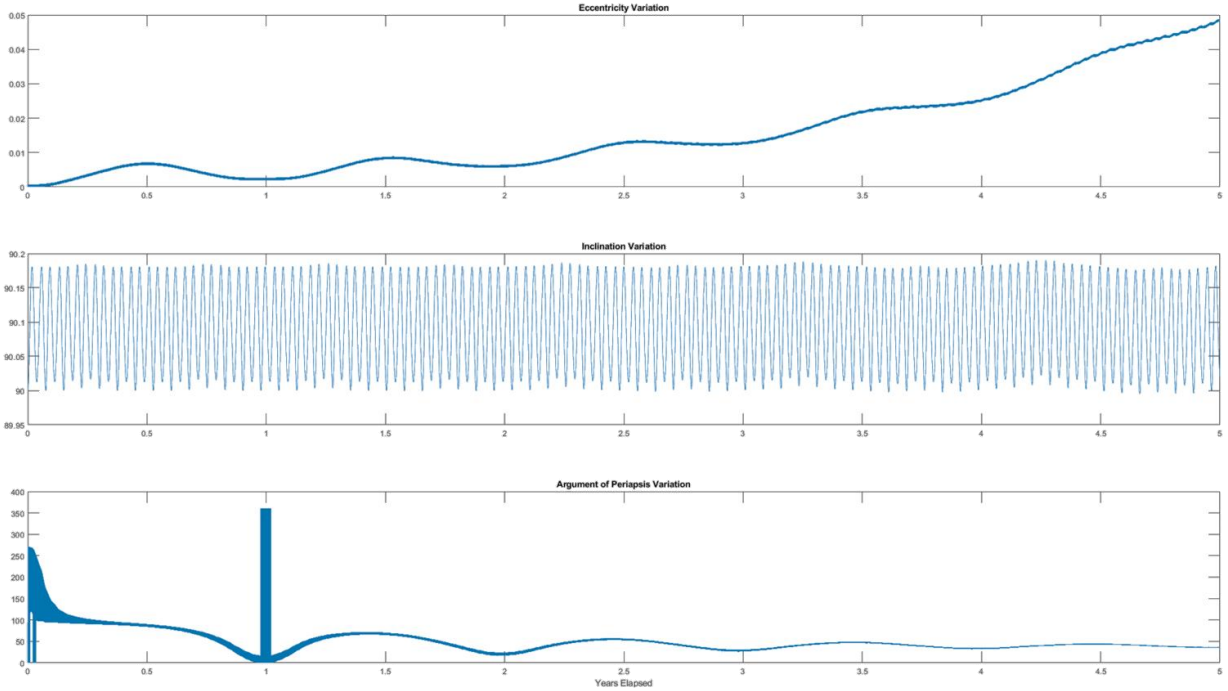

Figure 15: MATLAB Simulation of Orbital Parameter Variation for Orbit 2

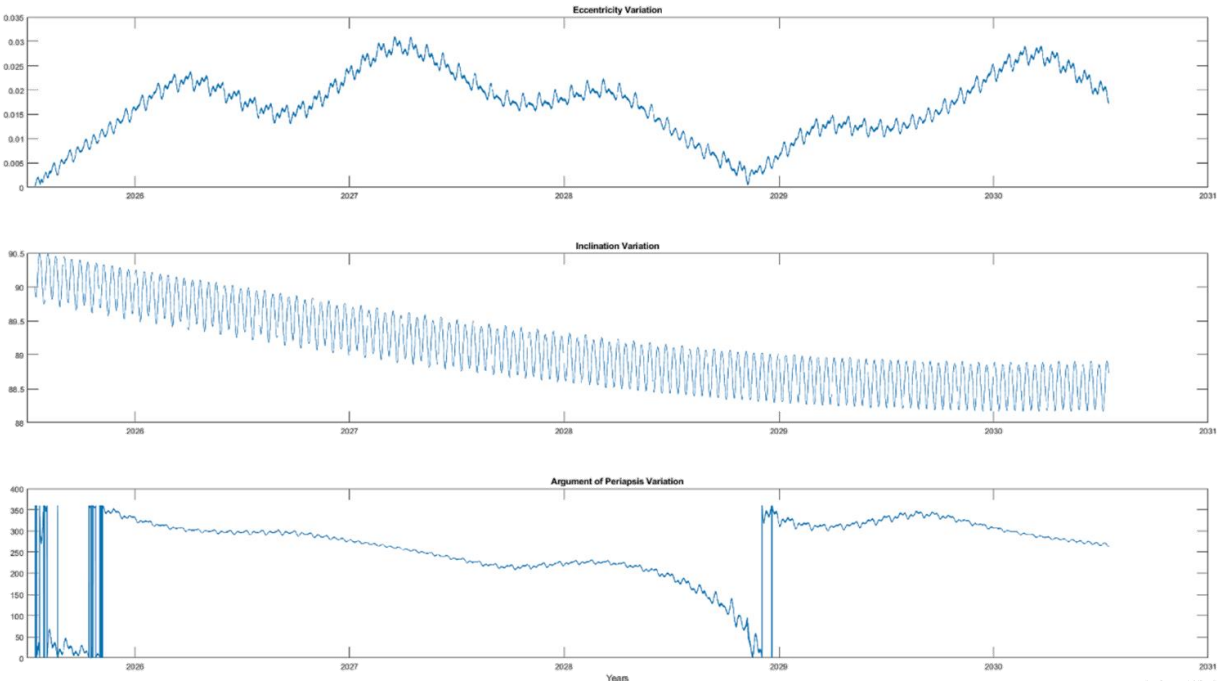

Figure 16: GMAT Simulation of Orbital Parameter Variation for Orbit 2

Copyright ©2020 by the authors. Published by the IAF, with permission and released to the IAF to publish in all forms.

A.3 - Orbit 3

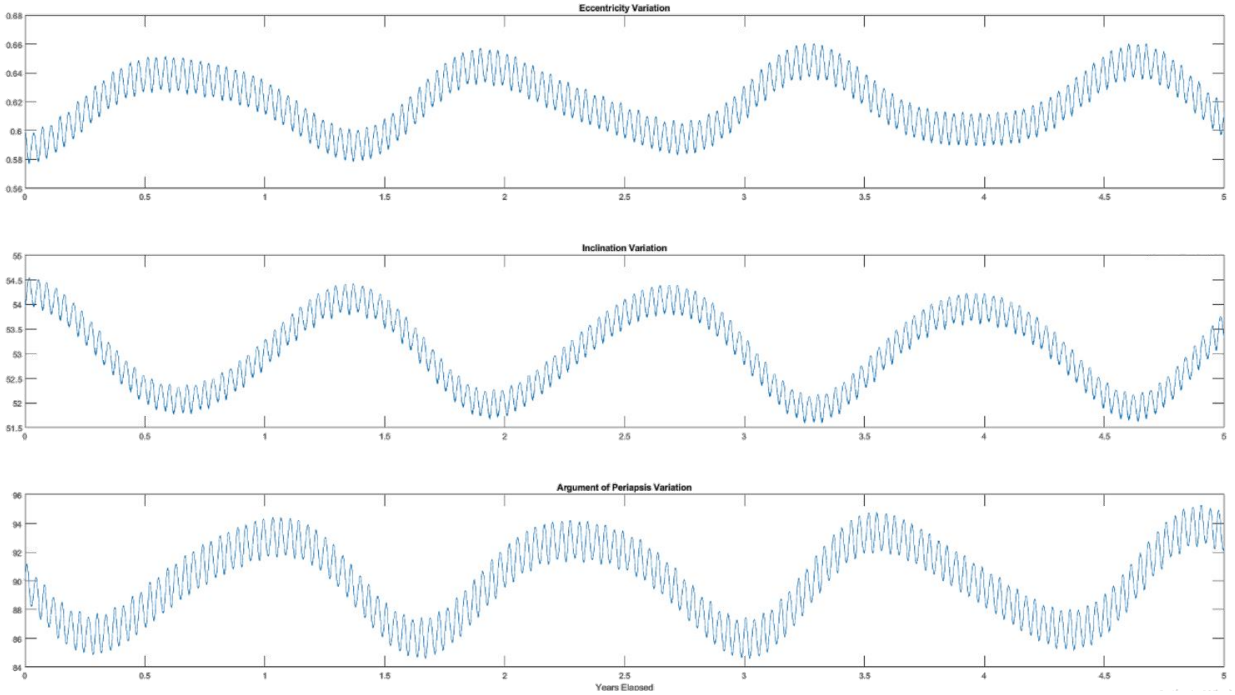

Figure 17: MATLAB Simulation of Orbital Parameter Variation for Orbit 3

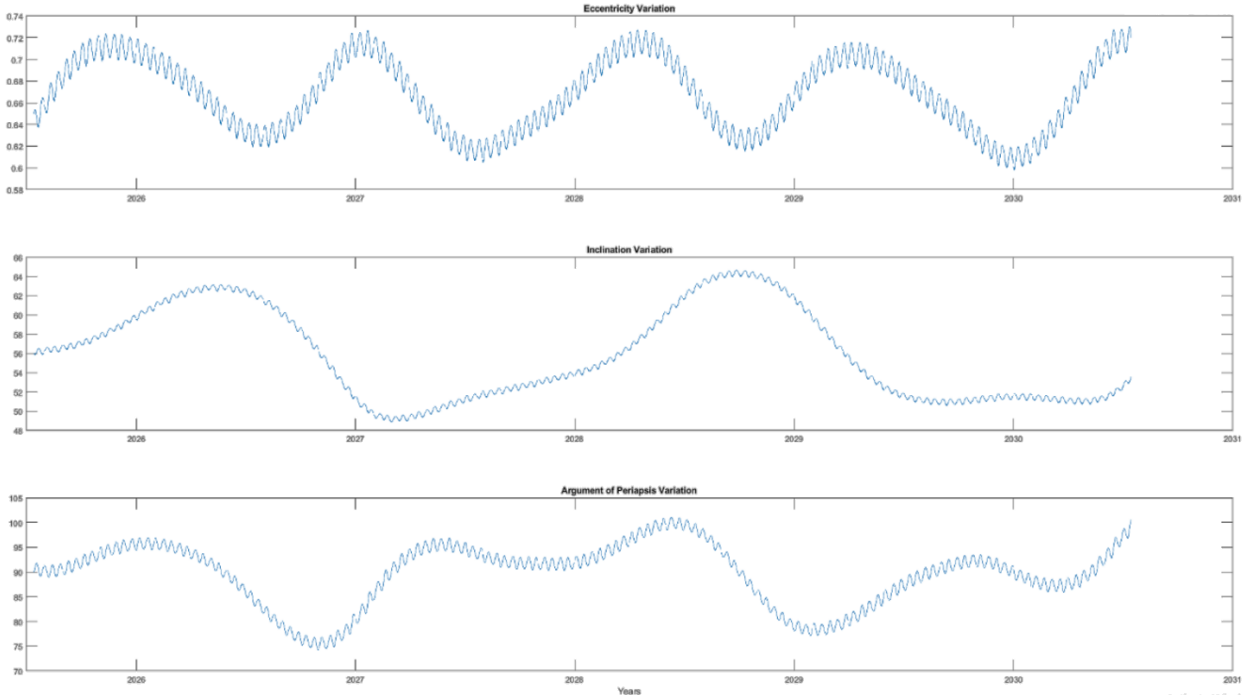

Figure 18: GMAT Simulation of Orbital Parameter Variation for Orbit 3

Copyright ©2020 by the authors. Published by the IAF, with permission and released to the IAF to publish in all forms.

A.4 - Orbit 4

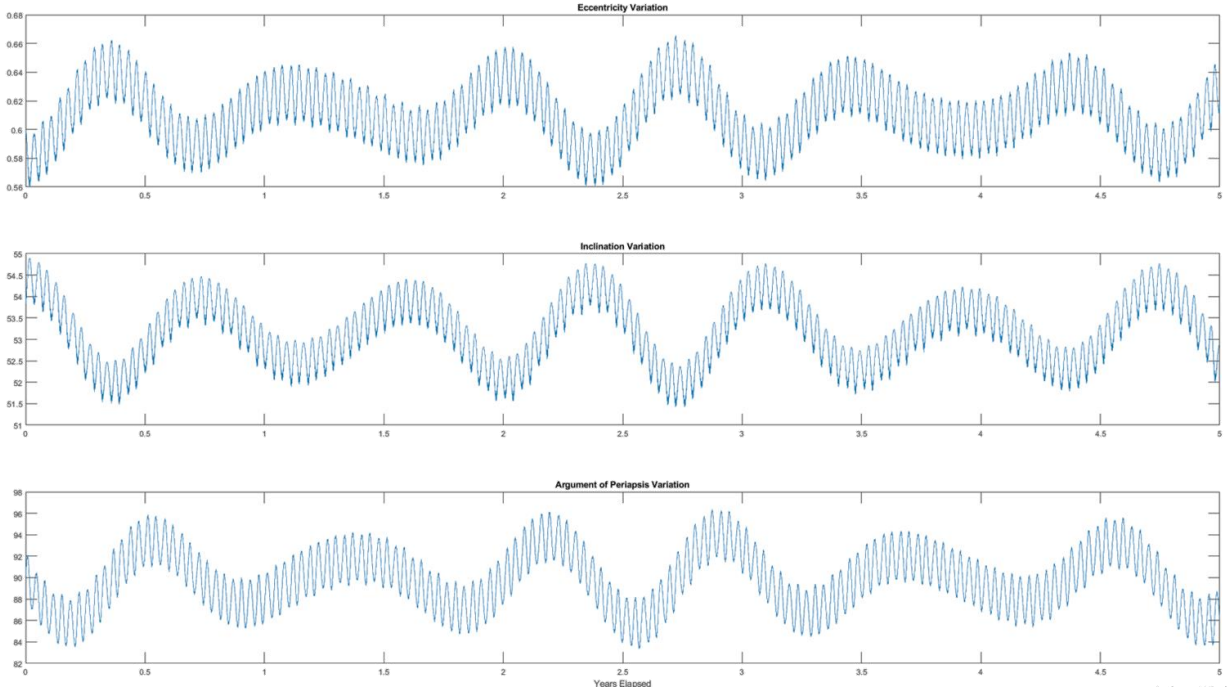

Figure 19: MATLAB Simulation of Orbital Parameter Variation for Orbit 4

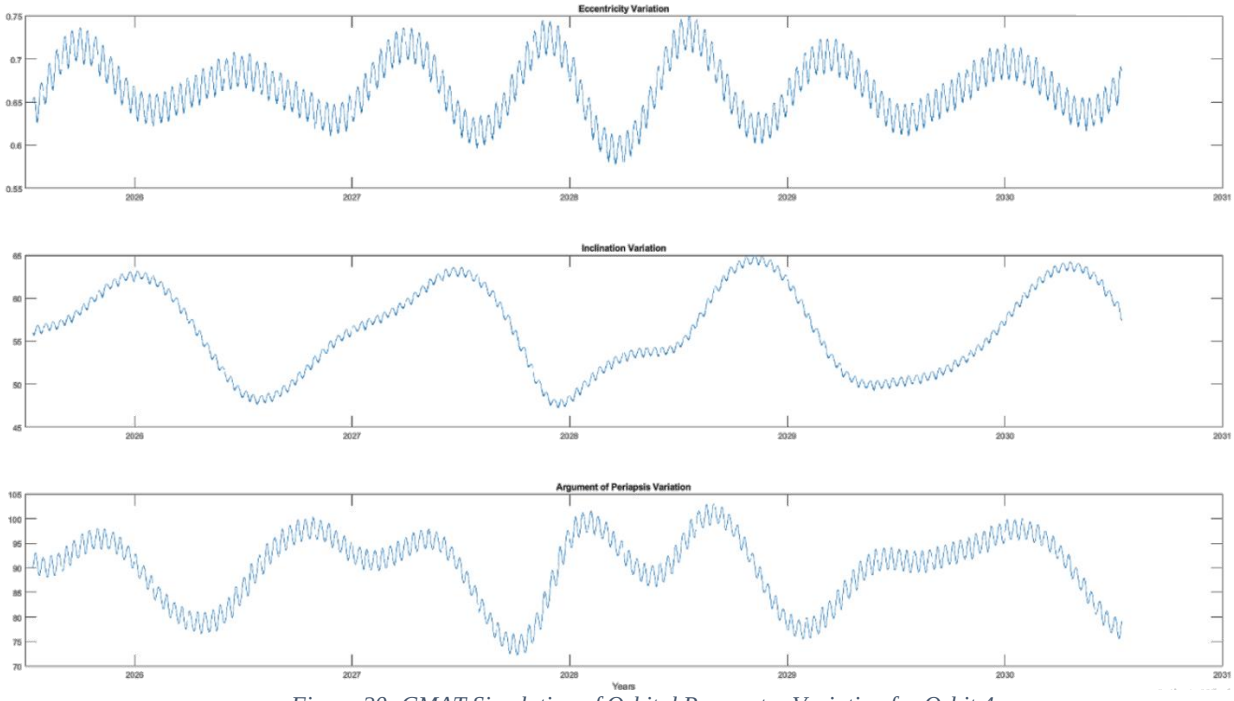

Figure 20: GMAT Simulation of Orbital Parameter Variation for Orbit 4

Copyright ©2020 by the authors. Published by the IAF, with permission and released to the IAF to publish in all forms.

References

[1] R. B.Malla and K. M.Brown, "Determination of temperature variation on lunar surface and subsurface for habitat analysis and design," *Acta Astronautica*, vol. 107, pp. 196-207, 2015.

[2] Z. Khan, A. Vranis, A. Zavoico, S. Freid and B. Manners, "Power System Concepts for the Lunar Outpost: A Review of the Power Generation, Energy Storage, Power Management and Distribution (PMAD) System Requirements and Potential Technologies for Development of the Lunar Outpost," in *Space Technology and Applications International Forum*, Albuquerque, New Mexico, 2006.

[3] P. E. Glaser, "Power from the Sun: Its Future," *Science*, vol. 162, pp. 857-861, 1968.

[4] C. Cougnet, E. S. (1), A. Celeste and L. Summerer, "SOLAR POWER SATELLITES FOR SPACE APPLICATIONS," in *55th International Astronautical Congress*, Vancouver, Canada, 2004.

[5] Strategic Missions and Advanced Concepts Office, "Solar Power Technologies for Future Planetary Science Missions," NASA, Pasadena, California, 2017.

[6] M. Arya, N. Lee and S. Pellegrino, "Ultralight Structures for Space Solar Power Satellites," in *3rd AIAA Spacecraft Structures Conference*, San Diego, California, 2016.

[7] J. C. Mankins and J. Howell, "Overview of the Space Solar Power Exploratory Research and Technology Program," in *35th Intersociety Energy Conversion Engineering Conference and Exhibit*, Las Vegas, Nevada, 2000.

[8] Swiss Space Centre, "IGLUNA," Swiss Space Centre, [Online]. Available: https://www.spacecenter.ch/igluna/. [Accessed 27 08 2020].

[9] NASA, "Reference Guide to the International Space Station," NASA, Washington, DC, 2010.

[10] Boeing Mediaroom, "Boeing Ships LightSquared's SkyTerra 1 Mobile Communications Satellite to Launch Site," Boeing Defense, Space & Security, 19 October 2010. [Online]. Available: https://boeing.mediaroom.com/2010-10-19-Boeing-Ships-LightSquareds-SkyTerra-1-Mobile-Communications-Satellite-to-Launch-Site.

[11] J. Amos, "Huge antenna launched into space," BBC News, 2010.

[12] W. C. Brown, "RECTENNA TECHNOLOGY PROGRAM: Ultra Light 2.45 GHz Rectenna and 20 GHz Rectenna," NASA, Cleveland, Ohio, 1987.

[13] NASA, "Orion Quick Facts," 4 August 2014. [Online]. Available: https://www.nasa.gov/sites/default/files/fs-2014-08-004-jsc-orion_quickfacts-web.pdf.

[14] W. Reynolds, "Architecture Analysis of Wireless Power Transmission for Lunar Outposts," Monterey, California, 2015.

[15] T. E. Bell, "Bizarre Lunar Orbits," 2006. [Online]. Available: https://science.nasa.gov/science-news/science-at-nasa/2006/06nov_loworbit/. [Accessed 31 March 2020].

[16] M. M. Mojarradi, G. Chattopadhyay, H. Manohara, T. A. Vo, H. Mojaradi, S. Y. Bae and N. Marzwell, "Scalable Millimeter Wave Wireless Power Receiver Technology for Space Applications," in *AIAA SPACE 2008 Conference & Exposition*, San Diego, California, 2008.

[17] S. Mizojiri and K. Shimamura, "Wireless power transfer via Subterahertz-wave," *Applied Sciences*, vol. 8, no. 12, 2018.

[18] K. Minakawa, K. Matsui, W. Komurasaki, Y. Hatakeyama, K. Okamoto, M. Suzuki, K. Shimamura, A. Mizushima, K. Fujiwara and H. Yamaoka, "Microstrip antenna and rectifier for wireless power transfar at 94GHz," in *IEEE Wireless Power Transfer Conference*, Taipei, Taiwan, 2017.

[19] H.-K. Chiou and I.-S. Chen, "High-Efficiency Dual-Band On-Chip Rectenna for 35- and 94-GHz Wireless Power Transmission in 0.13-□m CMOS Technology," *IEEE TRANSACTIONS ON MICROWAVE THEORY AND TECHNIQUES*, vol. 58, no. 12, 2010.

[20] T.-W. Yoo and K. Chang, "Theoretical and Experimental Development of 10 and 35 GHz Rectennas," *IEEE TRANSACTIONS ON MICROWAVE THEORY AND TECHNIQUES*, vol. 40, no. 6, 1992.

[21] W. C. Brown and E. E. Eves, "Beamed Microwave Power Transmission and its Application to Space," *IEEE TRANSACTIONS ON MICROWAVE THEORY AND TECHNIQUES*, vol. 40, no. 6, 1992.

[22] Z.-Q. Liu, H. Qiu, X. Li and S.-L. Yang, "Review of Large Spacecraft Deployable Membrane Antenna Structures," *Chinese Journal of Mechanical Engineering*, vol. 30, pp. 1447-1459, 2017.

[23] R. C. Hansen, "32 - Antennas," in *Reference Data for Engineers: Radio, Electronics, Computer, and Communications (Ninth Edition)*, Newnes, 2002, pp. 1-58.

Copyright ©2020 by the authors. Published by the IAF, with permission and released to the IAF to publish in all forms.

[24] A. Kasugai, K. Sakamoto, K. Takahashi, K. Kajiwara and N. Kobayashi, "Steady-state operation of 170 GHz–1 MW," *Nuclear Fusion*, vol. 48, 2008.

[25] D. Borodin, R. Ben-Moshe and M. Einat, "Design of 95 GHz gyrotron based on continuous operation copper solenoid with water cooling," *Review of Scientific Instruments*, vol. 85, 2014.

[26] Canon Electron Tubes & Devices, "Microwave Tubes / Power Grid Tubes - Gyrotrons," Canon Electron Tubes & Devices, 2020. [Online]. Available: https://etd.canon/en/product/category/microwave/gyrotron.html.

[27] C. Lei, S. Yu, H. Li, Y. Liu and Q. Zhao, "Design and numerical simulation of a 94 GHz gyrotron with gradually tapered cavity," *Qiangjiguang Yu Lizishu/High Power Laser and Particle Beams*, vol. 26, no. 2, 2014.

[28] J. M. Neilson, M. Read and R. L. Ives, "P3-4: Design and assembly of a permanent magnet gyrotron for active denial systems," in *IEEE International Vacuum Electronics Conference* , Monterey, California, 2010.

[29] AZUR SPACE Solar Power GmbH, "SPACE Solar Cells," AZUR SPACE Solar Power GmbH, 2019. [Online]. Available: http://www.azurspace.com/index.php/en/products/products-space/space-solar-cells.

[30] J. R. Wertz, D. F. Everett and J. J. Puschell, Space Mission Engineering: The New SMAD, Hawthorne, California: Microcosm Press, 2015.

[31] R. Pappa, G. Rose, T. Mann, J. Warren, M. Mikulas, T. Kerslake, T. Kraft and J. Banik, "Solar Array Structures for 300 kW-Class Spacecraft," in *Space Power Workshop*, Manhatten Beach, California, 2013.

[32] M. F. Ashby, Materials and the Environment: Eco-Informed Material Choice, Oxford: Butterworth-Heinemann, 2013.

[33] M. Ashby, "Material property data for engineering materials," Granta Design, Cambridge, UK, 2016.

[34] G. Filippi, M. Vasile, D. Krpelik, P. Z. Korondi, M. Marchi and C. Poloni, "Space systems resilience optimisation under epistemic uncertainty," *Acta Astronautica*, vol. 165, pp. 195-210, 2019.

[35] N. Lior, "Mirrors in the sky: Status, sustainability, and some supporting," *Renewable and Sustainable Energy Reviews*, vol. 18, no. 1, pp. 401- 415, 2013.

[36] K. W. Billman, W. P. Gilbreath and S. W. Bowen, "Introductory assessment of orbiting reflections for terrestrial power generation," NASA United States, California, 1977.

[37] M. Yang and C. Zhou, "Comparison of different strategies to realize highly reflective thin film coatings at 1064 nm," *Infrared Physics & Technology*, vol. 51, no. 6, pp. 572-575, 2008.

[38] L. Barron, "High-reflectance, sputter-deposited aluminum alloy thin thin films for micro-electro-mechanical systems," Rochester Institute of Technology, Rochester, 2005.

[39] D. Lichodziejewski and B. Derbès, "Bringing an Effective Solar Sail Design Toward TRL 6," Huntsville, Alabama, 2003.

[40] H. J. Kramer, "InflateSail," eoPortal, May 2019. [Online]. Available: https://directory.eoportal.org/web/eoportal/satellite-missions/i/inflatesail. [Accessed 10 november 2019].

[41] I. Cash, "CASSIOPeiA Solar Power Satellite," in *IEEE International Conference on Wireless for Space and Extreme Environments*, Montreal, Canada, 2017.

[42] I. Cash, "CASSIOPeiA – A new paradigm for space solar power," *Acta Astronautica*, vol. 159, pp. 170-178, 2019.